

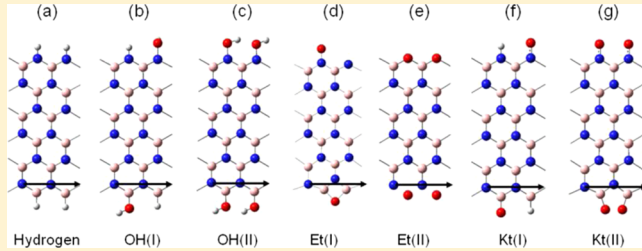
Effects of Edge Oxidation on the Structural, Electronic, and Magnetic Properties of Zigzag Boron Nitride Nanoribbons

Dana Krepel and Oded Hod*

Department of Chemical Physics, School of Chemistry, The Raymond and Beverly Sackler Faculty of Exact Sciences, Tel Aviv University, Tel Aviv 69978, Israel

 Supporting Information

ABSTRACT: The effects of edge chemistry on the relative stability and electronic properties of zigzag boron nitride nanoribbons (ZBNNRs) are investigated. Among all functional groups considered, fully hydroxylated ZBNNRs are found to be the most energetically stable. When an in-plane external electric field is applied perpendicular to the axis of both hydrogenated and hydroxylated ZBNNRs, a spin-polarized half-metallic state is induced, whose character is different than that predicted for zigzag graphene nanoribbons. The onset field for achieving the half-metallic state is found to mainly depend on the width of the ribbon. Our results indicate that edge functionalization of ZBNNRs may open the way for the design of new nanoelectronic and nanospintronic devices.



The recent experimental realization of atomically thin, long, and narrow strips of graphene, often referred to as graphene nanoribbons (GNRs)^{1–5} has triggered extensive experimental and theoretical investigations of their physical properties. Due to their unique structural, mechanical, electronic, and magnetic characteristics, GNRs have been identified as promising candidates for numerous potential applications including spintronic devices, gas sensors, and nanocomposite materials.^{6–9} The quasi-one-dimensional nature of GNRs results in the presence of reactive edges that may dominate their electronic and magnetic behavior.^{10,11} Specifically, when grown along the zigzag axis the resulting zigzag graphene nanoribbons (ZGNRs) present pronounced electronic edge states^{12–14} making them prone to covalent attachment of chemical groups that can significantly alter their electronic properties.^{5,15–21} Within the simplest edge passivation scheme, hydrogen terminated ZGNRs were shown to exhibit a spin polarized semiconducting ground state with bandgaps that vary with the ribbon width.¹⁴ This ground state is characterized by energetically degenerate α and β molecular spin orbitals that are spatially related via inversion symmetry. Here, opposite spin orientations localize at the two edges of the ZGNR and couple through the graphene backbone via an antiferromagnetic (AF) arrangement of spins on adjacent atomic sites. The application of an in-plane electric field, perpendicular to the ZGNR's axis, was shown to lift this bandgap degeneracy, thus creating a perfect spin filter where electrons carrying one spin flavor present metallic behavior whereas their opposite spin counterparts exhibit wide bandgap semiconductor characteristics.^{14,22}

Hexagonal boron nitride (*h*-BN) is the inorganic analogue of graphite. The two materials are isoelectronic, and their hexagonal lattices are isomorphic. In analogy to graphene, a

single layer of *h*-BN has an equal number of sp^2 hybridized B and N atoms, which are covalently bonded in an alternating pattern. Nevertheless, due to the differences in electron affinities of the boron and nitrogen atoms, the B–N bonds have a considerable ionic character. This results in major differences both in their optimal interlayer stacking (graphite presents the Bernal ABA stacking whereas *h*-BN has the antieclipsed AA'A stacking)²³ and in their electronic properties (graphene is a semimetal whereas *h*-BN is an insulator).²⁴

Because of these characteristics, *h*-BN has also attracted significant attention from the scientific community.^{24–32} With this respect, the electronic and magnetic properties of boron-nitride nanoribbons (BNNRs) with bare edges have been thoroughly investigated providing theoretical evidence that they are magnetic semiconductors with bandgaps that decrease with increasing ribbon width.^{33,34} Half-metallicity has also been predicted to occur in zigzag BNNRs (ZBNNRs) with fluorine edge-decoration,^{35,36} hydrogenation,³⁷ and Stone-Wales defects.³⁸ Furthermore, it was shown that terminating both the B and the N zigzag edges with oxygen and sulfur atoms gives rise to metallic behavior in these systems.³⁹

Here, we present a first-principle computational study of the effects of edge oxidation on the relative stability, electronic properties, and half-metallic nature of ZBNNRs. To this end, we consider six different oxidation schemes of a 1.37 nm wide ZBNNR as shown in Figure 1. We note these oxidation schemes in accordance to their GNR counterparts, namely,⁵ partial hydroxylation (panel b, OH(I)), full hydroxylation (panel c, OH(II)), etheration schemes (panel d, Et(I), and e,

Received: October 9, 2013



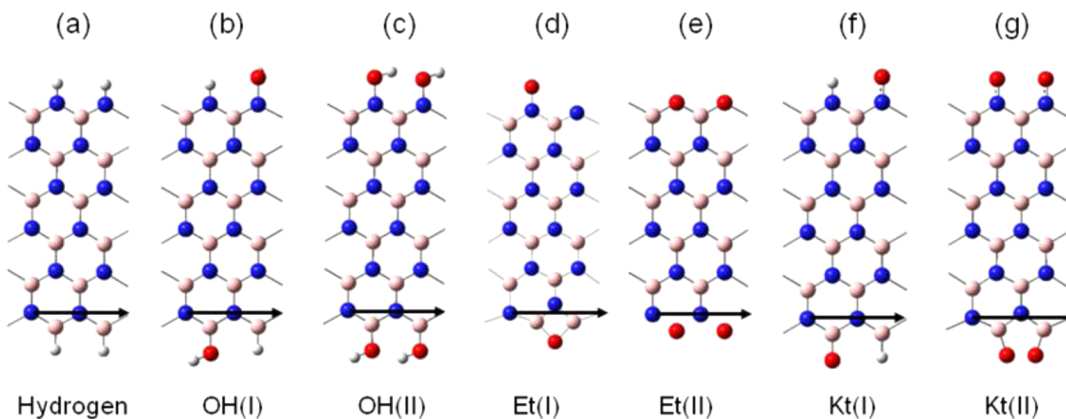


Figure 1. Optimized unit-cell geometries of different edge oxidation schemes studied in this work. The presented structures were obtained at the HSE/6-31G** level of theory. Color code: red, oxygen atoms; blue, nitrogen atoms; pink, boron atoms; gray, hydrogen atoms. Arrows represent the periodic direction of the ZBNRs.

Et(II)), partial ketonation (panel f, Kt(I)), and full ketonation (panel g, Kt(II)).

Our calculations have been carried out utilizing the GAUSSIAN suite of programs.⁴⁰ Spin-polarized calculations have been performed within the local density approximation (LDA), the generalized gradient approximation of Perdew et al. (PBE),^{41,42} and the screened-exchange hybrid functional developed by Heyd, Scuseria, and Ernzerhof (HSE)^{43–46} of density functional theory (DFT). We note that the latter functional approximation has been shown to reproduce experimental optical bandgaps of bulk semiconductors and to describe the physical properties of a wide variety of materials, including carbon nanotubes and graphene and its derivatives, with much success.^{5,47–51} Unless otherwise stated the double- ζ polarized 6-31G** Gaussian basis set was used.⁵² Basis set convergence tests have been performed (see Figure S1 in the Supporting Information and ref 33) indicating that the relative structural stability values and calculated bandgaps are converged to within 5% and 2%, respectively.

We start by discussing the optimized structures of the various systems considered. In Figure 1 we present the relaxed geometries obtained at the HSE/6-31G** level of theory. For the hydrogen terminated system (Figure 1a) we find that the N–H bonds (1.01 Å) are somewhat shorter than the B–H bonds (1.12 Å). Upon partial hydroxylation of both edges (Figure 1b) the hydroxyl group attached to the boron edge remains in the plane of the ribbon whereas the hydroxyl group bonded to the nitrogen edge rotates to become perpendicular to the basal plane of the system. For the fully hydroxylated system (Figure 1c) the formation of a network of hydrogen bonds between adjacent OH groups causes the substituents to remain in the plane of the ribbon similar to the case of fully hydroxylated GNRs.^{5,53} When both edges are partially decorated with ether groups (Figure 1d), the optimization procedure results in a structure where the boron edge exhibits an ether-like configuration whereas the nitrogen edge obtains a partial ketone-like structure. In Figure 1e both edges are fully functionalized with ether-like groups where oxygen atoms replace the edge boron and nitrogen atoms. Here, the geometry optimization maintains the general structure while elongating the N–O bonds (1.49 Å) as compared to the B–O (1.39 Å) counterparts. A somewhat different picture arises upon partial ketonation (Figure 1f) where the obtained N–O bonds (1.26 Å) are shorter than the B–O bonds (1.40 Å). Finally, when

covering both edges with ketone-like groups, the optimized structure presents a ketonated nitrogen edge and a peroxide-like structure on the boron edge (Figure 1g). For simplicity, we name the different structures according to the original functionalization scheme prior to geometry optimization.

Next, we study the relative stability of the different oxidized ribbons. As these structures have different chemical compositions, the cohesive energy per atom does not provide a suitable measure for the comparison of their relative stabilities. Therefore, we adopt the approach used in refs 5, 47, and 54 where one defines a Gibbs free energy of formation δG for a BNNR as follows:

$$\delta G(\chi_H, \chi_O) = E(\chi_H, \chi_O) - \chi_H \mu_H - \chi_O \mu_O - \chi_{BN} \mu_{BN} \quad (1)$$

where $E(\chi_H, \chi_O)$ is the cohesive energy per atom of a BNNR with given composition and dimensions, χ_i is the molar fraction of atom i ($i = H, O$, or BN couple) in the ribbon satisfying the relation $\sum \chi_i = 1$, and μ_i is the chemical potential of the constituent at a given state. We choose μ_H as the binding energy per atom of the singlet ground state of the hydrogen molecule, μ_O as the binding energy per atom of the triplet ground state of the oxygen molecule, and μ_{BN} as the cohesive energy per BN couple of a single two-dimensional BN sheet, all calculated at the same level of theory as $E(\chi_H, \chi_O)$. This definition allows for an energy comparison between oxidized nanoribbons with different compositions, where negative values represent stable structures with respect to the constituents. For all oxidation schemes considered, we compared the closed-shell singlet spin state with the triplet spin state in order to identify the lowest energy spin configuration of each system.

In Figure 2 we present the relative stabilities of the different oxidized ZBNRs studied using the HSE functional approximation (LDA and PBE results are presented for comparison in Figure S2 of the Supporting Information). As can be seen, the fully hydrogenated ribbon as well most of the oxidized ribbons considered are found to be less stable than their corresponding constituents. Conversely, both hydroxylation schemes lead to considerable energetic stabilization of the ribbon's structure. We find that the most stable structure corresponds to the full edge-hydroxylation scheme (Figure 1c). As mentioned above, this enhanced stability is attributed to the hydrogen bonds formed between adjacent edge hydroxyl groups and is consistent with previous calculations on edge oxidized ZGNRs.⁵ Furthermore, we note that for the fully hydrogenated

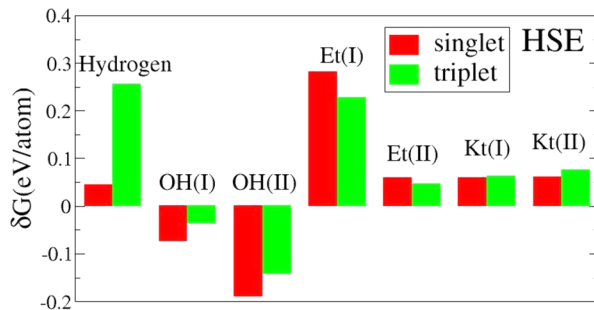


Figure 2. Ground state relative stabilities of the different oxidized systems studied (see Figure 1) obtained via eq 1 at the HSE/6-31G** level of theory. Negative values indicate stable structures with respect to the constituents. Results of the singlet and triplet spin state calculations are presented in red and green bars, respectively.

system, as well as for both hydroxylated structures, the closed-shell singlet spin state is more energetically stable than the corresponding triplet state.

Having identified the most stable edge oxidation scheme, we now turn to study the electronic properties of the oxidized ZBNNRs considered. In Figure 3 we present the bandgaps,

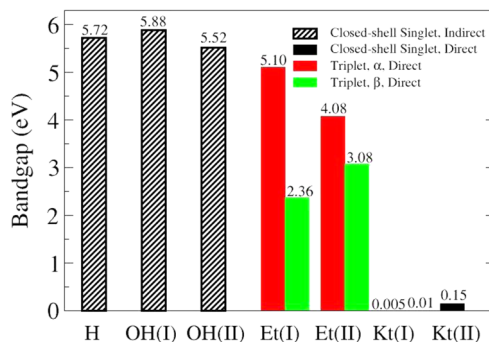


Figure 3. Bandgap response to different oxidation schemes studied at the HSE/6-31G** level of theory. The singlet spin state is represented by black bars whereas the triplet spin state is represented by red (α spin electrons) and green (β spin electrons) bars. Full and striped bars represent direct and indirect bandgaps, respectively.

calculated as energy differences between the lowest unoccupied (LUCO) and highest occupied (HOCO) crystalline Kohn–Sham orbitals, using the HSE functional approximation (LDA and PBE results are presented for comparison in Figure S3 of the Supporting Information). Our calculations show that the bandgap obtained for the fully hydrogenated system is 5.72 eV using the HSE functional and 4.24 eV using the PBE approximation, which is in good agreement with previous studies of similar structures (5.56 eV³³ and 4.26 eV,³⁹ respectively). Interestingly, the two hydroxylation schemes present relatively small (~0.2 eV) modifications of the bandgap preserving the system's insulating character while maintaining the indirect nature of the bandgap. Furthermore, the lower hydroxyl density is found to slightly increase the bandgap whereas the higher hydroxyl density slightly decreases the bandgap with respect to the fully hydrogenated ZBNNR.

Markedly, the bandgap response toward the other edge oxidation schemes is highly diverse. Here, the triplet ground states of the Et(I) and Et(II) oxidation schemes lift the spin degeneracy such that for Et(I) the bandgap of one spin flavor is reduced by ~11% (0.62 eV) while the bandgap of the opposite

spin electrons drops by 59% (3.36 eV). For the Et(II) oxidation scheme both up and down spin bandgaps reduce by ~62%, thus turning the system into a wide bandgap semiconductor. For the Kt(I) and Kt(II) structures the HSE bandgaps further decrease turning the system metallic for the Kt(I) structure and a narrow bandgap semiconductor for the Kt(II) system. Notably, all these oxidation schemes, most of which are comparable in stability to the edge hydrogenated system, result in direct bandgap materials thus demonstrating that edge chemistry can be used as an efficient control scheme for tailoring the electronic properties of ZBNNRs.

In order to gain better understanding of the varied influence of the different oxidation schemes on the electronic properties of the ZBNNR, we performed band structure and density of states (DOS) analysis.⁵⁵ In Figure 4 we present the band structures along with the full DOSs (FDOS) and the partial DOSs (PDOS) of the B and N edges for the hydrogenated, hydroxylated, and a representative ketonated ZBNNRs. The edge PDOSs include only the contributions of the oxidation functional groups covalently bonded to the relevant edge atoms.

When examining the electronic properties of the hydrogen terminated system (Figure 4a), it is found that the HOCO and LUCO are associated with the central section of the ZBNNR. The N-edge contribution appears ~2 eV above the conduction band minimum (CBM) whereas the B-edge DOS appears ~2.5 eV below the valence band maximum (VBM). Partial hydroxylation (Figure 4b) results in relatively minor changes of the HOCO and LUCO dispersion relations. From the PDOS analysis it is found that the N-edge now contributes some DOS to the low lying valence bands while the B-edge develops DOS at the high lying conduction bands. When the system is fully hydroxylated (Figure 4c), qualitative changes in the HOCO and LUCO dispersion relations, including the location of the VBM and CBM, are evident. Here, the N-edge is found to contribute DOS at the HOCO and near the LUCO and the B-edge gains some DOS above the LUCO band. It should be noted that a similar picture appears for the α spin state of the less stable Et(I), Et(II), and Kt(II) oxidation schemes (see Supporting Information Figure S4), whereas the β spin state of both schemes presents relatively flat bands in the mid-gap area. PDOS analyses reveal these bands are contributed from the N-edge.

The partial ketonation scheme is found to p-dope the system by shifting the Fermi energy into the valence band (Figure 4d). The screened hybrid HSE functional approximation predicts a small (~0.01 eV) direct bandgap whereas both the PBE and the LDA functionals predict metallic behavior. Here, both ketonated B- and N-edges present pronounced DOS at the Fermi energy with clearly evident qualitative changes of the low energy band structure.

Similar to the case of GNRs, the effects of edge chemistry on the electronic properties of ZBNNRs is expected to alter their response toward the application of external fields. Previous studies have shown that bare ZBNNRs may present a rich spectrum of electronic characteristics ranging from metallic through half-metallic to semiconducting under the influence of external electric fields.³³ Thus, it would be interesting to investigate whether edge oxidation may be used to further control the response of ZBNNRs to such external perturbations. In what follows, we focus the discussion on the most stable (hydroxylated) decoration scheme while using the hydrogenated system as a reference.

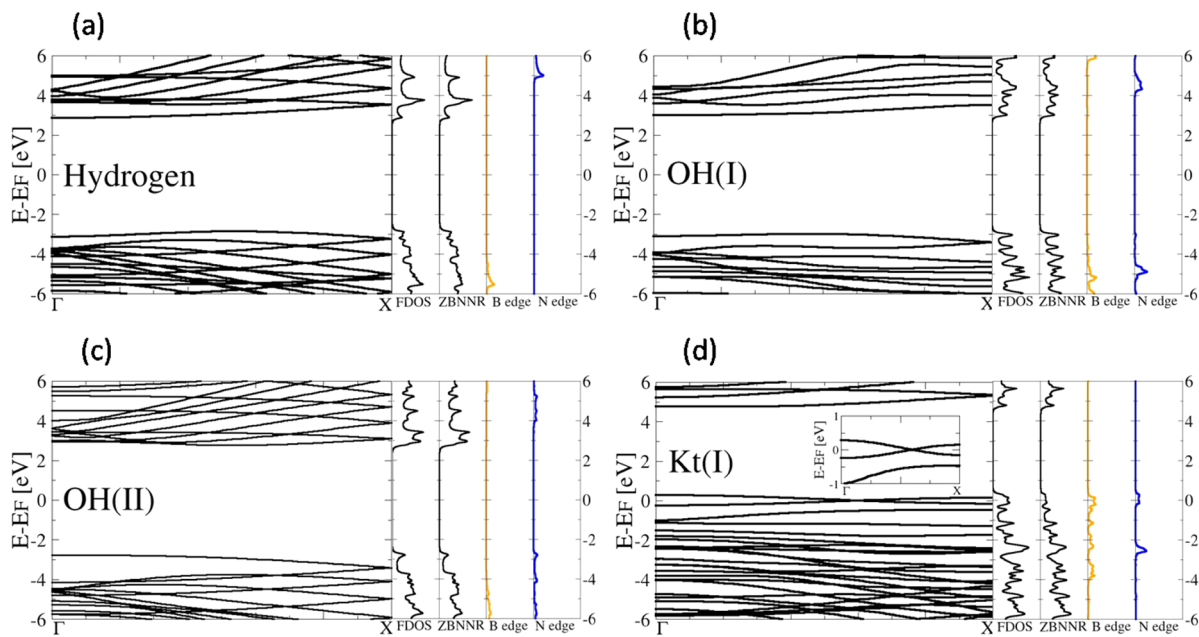


Figure 4. Band-structures, FDOS, and PDOS of the (a) hydrogen terminated; (b) partially hydroxylated (OH(I) scheme); (c) fully hydroxylated (OH(II) scheme); and (d) partially ketonated (Kt(I) scheme) ZBNNR as calculated at the HSE/6-31G** level of theory. Fermi energies of all diagrams are set to zero. Inset of panel (d): zoom-in on the band-structure in the range of $-1.0\text{--}1.0$ eV around the Fermi energy.

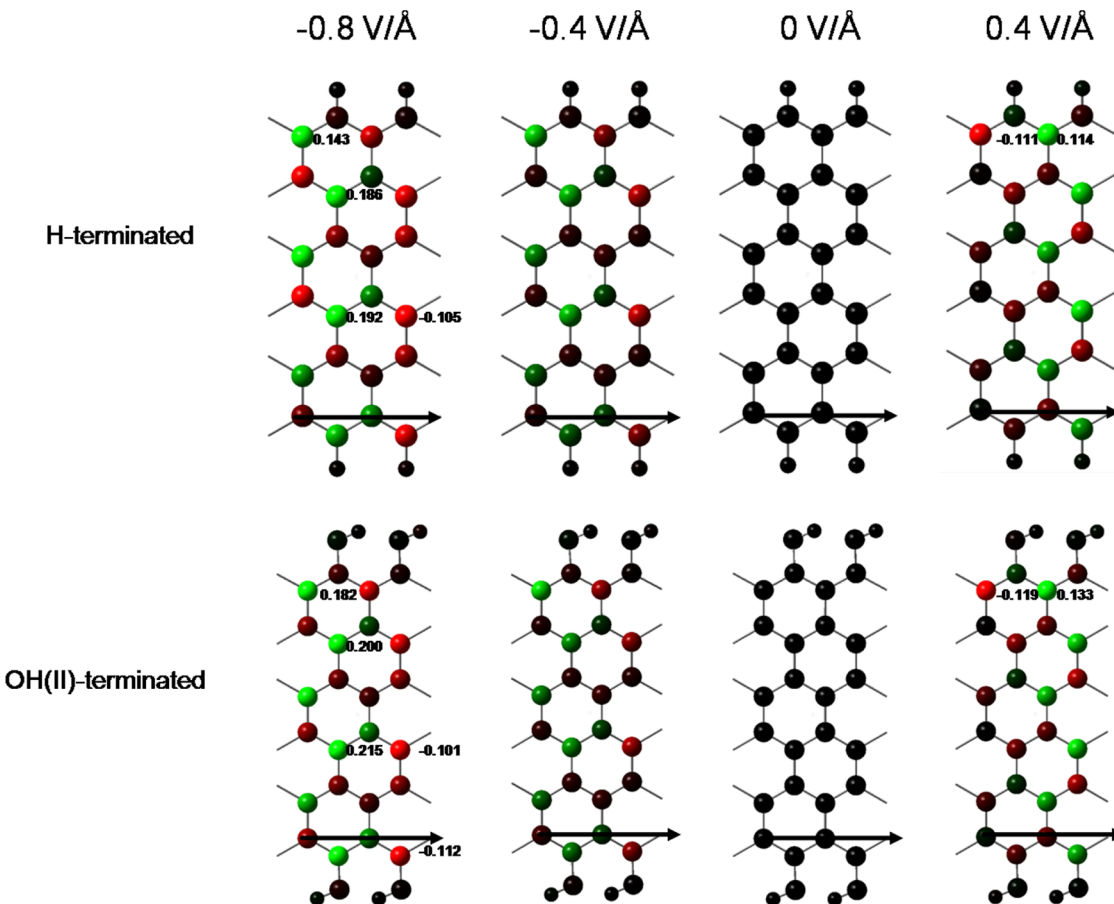


Figure 5. Ground state Mulliken atomic spin polarization calculated at the HSE/6-31G** level of theory for the hydrogenated (upper panels) and fully hydroxylated (lower panels) ZBNNRs at various external electric field intensities. Color code: red, α spin excess; green, β spin excess. Mulliken spin range is set to ± 0.1 in all panels. Representative Mulliken spin values are given for completeness. Arrows represent the periodic direction of the ZBNNRs.

To this end, we present in Figure 5 the ground state Mulliken atomic spin polarizations of the hydrogenated and the fully hydroxylated ZBNRs obtained at the HSE/6-31G** level of theory at various in-plane electric field intensities applied perpendicular to the main axis of the ribbons. Since ZBNRs lack mirror symmetry with respect to their central axis, not only the intensity but also the direction of the field has influence on the electronic properties of the system. Therefore, we consider both positive (pointing from the B- to the N-edge) and negative (pointing from the N- to the B-edge) electric fields. Opposite to the case of ZGNRs, where the ground state magnetization decreases with increasing external field intensity,⁵ here, in the absence of an external field, the ZBNRs are found to be nonmagnetic and the application of the external electric field induces spin polarization, regardless of its direction, both in the hydrogenated and the fully hydroxylated systems. As can be seen in Figure 6, a quadratic-like decrease in

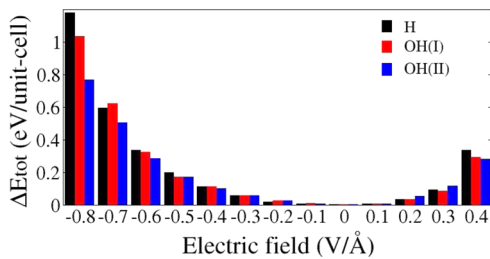


Figure 6. Energy differences between closed-shell and open-shell singlet spin state as function of external electric field intensity for the H, OH(I), and OH(II) edge decoration schemes obtained at the HSE/6-31G** level of theory.

the energetic stability of the closed-shell singlet spin state with respect to its open-shell counterpart is obtained with increasing field intensities. Remarkably, energy differences exceeding 1.1 eV/unit cell were obtained for the strongest external field considered of $-0.8 \text{ V}/\text{\AA}$ for the hydrogen terminated ZBNR. The partially and fully hydroxylated systems presented energy differences of 1.0 and 0.7 eV/unit cell, respectively, at this field intensity. For a positive field intensity of $0.4 \text{ V}/\text{\AA}$ we find that the replacement of edge hydrogen atoms with hydroxyl groups somewhat reduces the relative energetic stability of the open-shell singlet spin state.

With the understanding that an external electric field can drastically change the magnetic character of ZBNRs we now turn to discuss its influence on their electronic properties. In Figure 7 the band gap of hydrogenated and hydroxylated ZBNRs as a function of the external field intensity is presented. As can be seen, at relatively low intensities the bandgap associated with both α and β spin electrons are

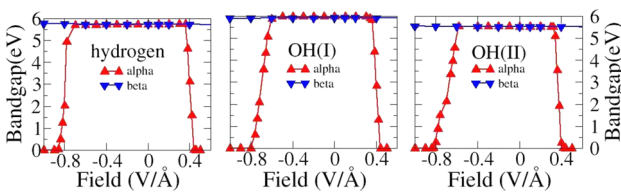


Figure 7. Spin polarized band gap as a function of the external electric field intensity of the hydrogenated (left panel) and partially (middle panel) and fully (right panel) edge-hydroxylated ZBNRs obtained at the HSE/6-31G** level of theory.

insensitive to the application of the external electric field. At a certain critical field strength, that varies with the edge passivation scheme, the α bandgap rapidly drops to zero while the β bandgap remains intact resulting in a half-metallic state. Interestingly, unlike the case of ZGNRs, the half-metallicity onset field in ZBNRs is weakly dependent on the edge hydroxylation scheme. Nevertheless, a careful examination reveals that the half-metallicity onset field is different for the positive and negative field directions. This may be rationalized by the fact that the B- and N-edges of the ZBNR are oppositely charged and therefore an inherent positive electric field is induced in the system. Hence, at the positive direction a lower external field intensity is required to induce half-metallicity.

In order to better understand the origin of the field induced half-metallic state observed in the ZBNRs studied we plot in Figure 8 the α electrons band structure along with the full α DOS and the B- and N-edges PDOs of the hydrogen terminated ZBNR at various electric field intensities. We note that the band structure associated with the β electrons is virtually insensitive to the external electric field in the intensity regime studied. As discussed above, in the absence of an external electric field the ground state of the system is of closed-shell insulating character with a wide HSE bandgap of 5.72 eV. At a field intensity of $-0.8 \text{ V}/\text{\AA}$ two energy bands originating from the field-less conduction band penetrate the bandgap region with a parabolic-like dispersion relation thus considerably reducing the value of the bandgap. The partial DOS analysis reveals that these bands are associated with the central section of the ribbons and not with its edges, consistent with the Mulliken spin polarization plots presented in Figure 5. As the field intensity is further increased to $-0.9 \text{ V}/\text{\AA}$ one of the two parabolic energy bands crosses the Fermi energy and the system becomes half-metallic. The main influence of the external field on the edge DOS is an upshift with respect to the Fermi energy. A similar qualitative picture with some quantitative differences is obtained when reversing the direction of the externally applied electric field. We note that similar results are obtained for the fully hydroxylated systems (see Supporting Information Figure S5). This behavior is completely different from that observed in ZGNRs where a field induced half-metallic state is achieved due to opposite local gating of the edge α and β spin DOSs.¹⁴

Finally, to verify the general nature of our results we have performed similar calculations on hydrogenated and hydroxylated ZBNRs of different widths. Previous studies of different spin states of bare BNNRs suggested that the energy difference between different spin states should vanish above a certain ribbon width.³³ Furthermore, the onset field for achieving a half-metallic state was shown to somewhat decrease with increasing bare ribbon width.

Here, we perform calculations on three edge decorated unit-cells of consecutive widths. We annotate these unit-cells by $(N \times M)$ where N stands for the number of zigzag chains along the width of the ribbon and M for the number of boron–nitride pair chains along its zigzag edge. Using this notation we study the (4×4) and (8×4) unit-cells and compare the result to those presented above for the (6×4) unit cell (see Figure 9), thus creating ribbons of the following widths: 0.94 nm, 1.37 nm, and 1.81 nm.

To study the influence of the width of the ribbons on their relative energetic stability we repeat the analysis performed above according to eq 1 for the edge-hydrogenated and partially

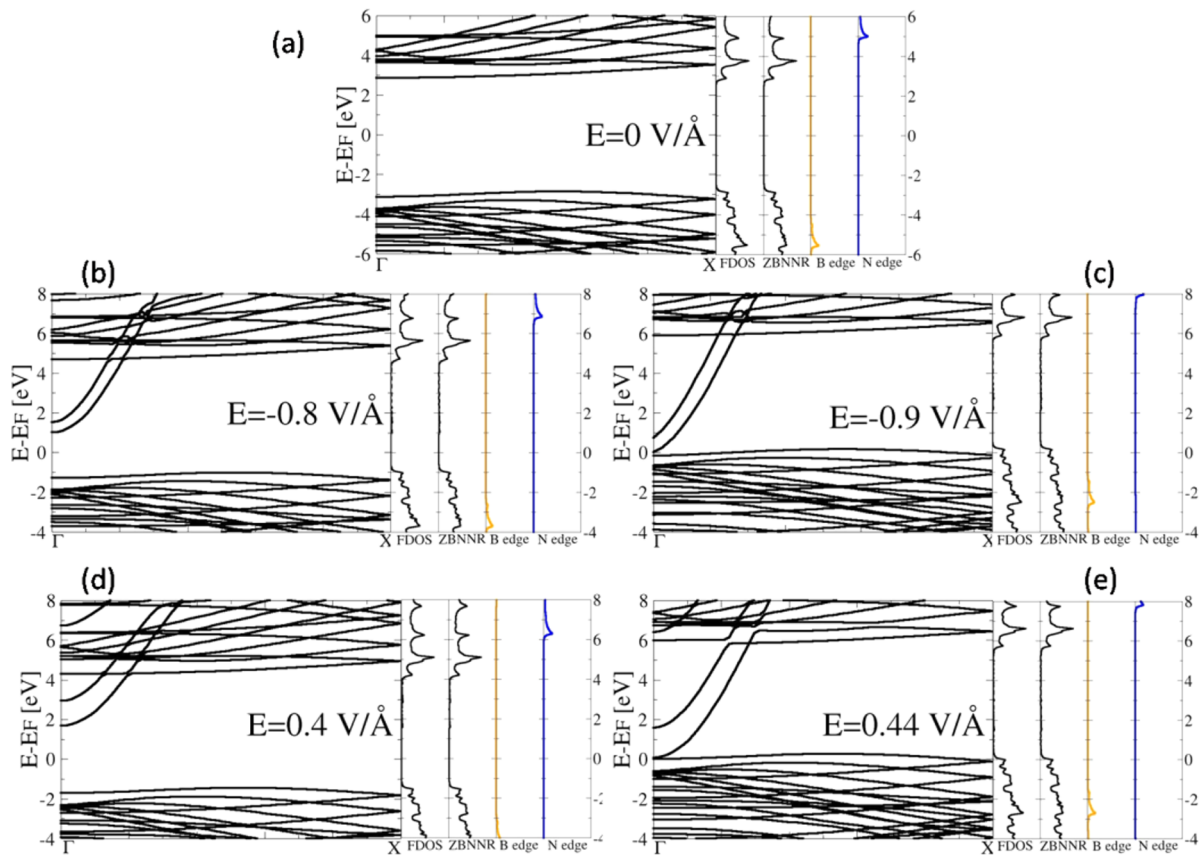


Figure 8. Band-structures, FDOS, and PDOS of the α spin state of the H-terminated ZBNNR at the following fields: (a) $0 \text{ V}/\text{\AA}$, (b) $-0.8 \text{ V}/\text{\AA}$, (c) $-0.9 \text{ V}/\text{\AA}$, (d) $+0.4 \text{ V}/\text{\AA}$, and (e) $+0.44 \text{ V}/\text{\AA}$ as calculated at the HSE/6-31G** level of theory. Fermi energies of all diagrams are set to zero.

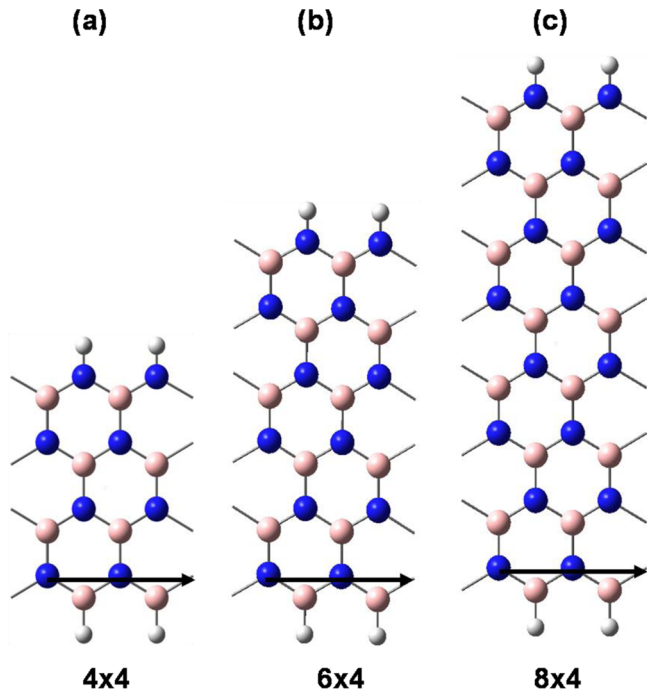


Figure 9. Schematic diagrams of the hydrogenated (a) (4×4) , (b) (6×4) , and (c) (8×4) ZBNNRs unit-cells. Arrows represent the periodic direction of the ZBNNRs.

and fully hydroxylated ribbons of various widths. The results for the different unit-cell dimensions are summarized in Figure 10.

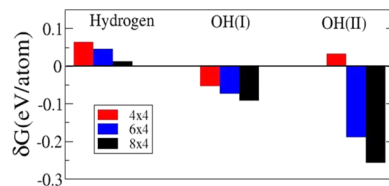


Figure 10. Relative stabilities of the H, OH(I), and OH(II) oxidation schemes (see Figure 1) as a function of ZBNNR width obtained via eq 1 at the HSE/6-31G** level of theory and the closed-shell singlet spin state. Negative values indicate stable structures with respect to the constituents.

We find that increasing the width of the ribbon results in an increase in its stability while generally maintaining the relative stability ordering of the three edge-decoration schemes.

The width of the ribbon was also found to influence its response toward the application of an external electric field. In Figure 11 we compare the bandgap dependence on the field intensity for the three ribbon widths considered with hydrogen and hydroxyl edge decoration. As can be seen, all systems considered present a similar zero-field bandgap of $5.5\text{--}6 \text{ eV}$. Nevertheless, upon the application of a positive external field the onset of half-metallicity shifts toward higher field intensities as the width of the ribbon is increased. An opposite picture arises for the negative field direction where the onset of half-metallicity shifts toward lower field intensities with increasing ribbons width. A similar behavior was also found in both hydrogen terminated ZGNRs and bare ZBNNRs.^{14,33} This width dependence may be explained using the simple model discussed above according to which the charge polarization

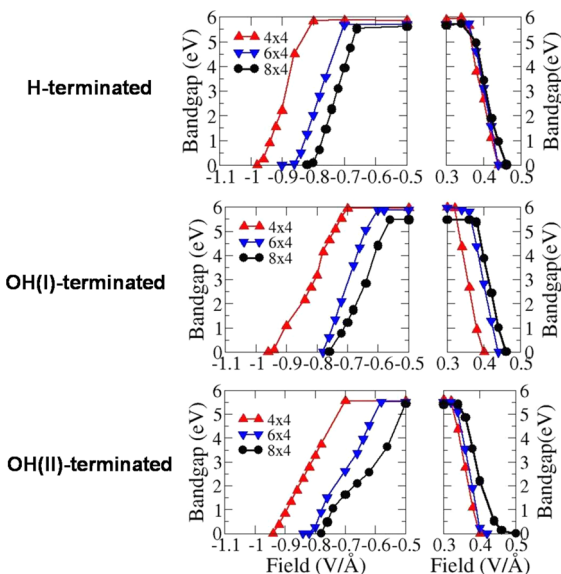


Figure 11. α spin bandgaps as a function of the field intensity and direction of the hydrogenated (upper panels) and partially (middle panels) and fully (lower panels) hydroxylated ZBNNRs of varying width obtained at the HSE/6-31G** level of theory.

between the B- and N-edges forms an intrinsic field that enhances or reduces the effect of the external field depending on its direction. As the width of the ribbon increases, the onset field intensity to obtain a half-metallic state in the negative (positive) direction is decreased (increased). This indicates that the intrinsic effective field decreases with increasing ribbon width. Nonetheless, we find that the qualitative nature of the response is similar for all systems studied, thus further supporting the general nature of our predictions.

In summary, we have studied the relative stability, electronic properties, and response to external electric field perturbations of ZBNNRs with various edge-oxidation schemes. It was found that chemical functionalization of the edges may considerably influence the relative stability of the system. Among all functional groups considered the fully hydroxylated ZBNNR was found to be the most energetically stable. This stability was found to enhance with increasing ribbon width. The influence of edge-functionalization on the ground state electronic structure was found to strongly depend on the chemical nature of the decorating group, where electronic character ranging from insulating to metallic was obtained for different oxidation schemes. The application of an external in-plane electric field perpendicular to the axis of edge-hydrogenated and hydroxylated ZBNNRs was found to induce a spin-polarized half-metallic state, whose nature is completely different than that observed in ZGNRs. The onset field for achieving the half-metallic state was found to mainly depend on the width of the ribbon with moderate sensitivity toward edge hydroxylation. Our results indicate that edge functionalized ZBNNRs should present novel electronic and magnetic properties that may open the way for the design of new nanospintronic devices.

ASSOCIATED CONTENT

Supporting Information

Effects of choice of basis set and functional approximation on the calculated relative stability and bandgaps. Band-structures, FDOSSs, and PDOSSs of the Et(I), Et(II), and Kt(II) systems in the absence of an electric field and of the OH(II) system at

various electric field intensities. This material is available free of charge via the Internet at <http://pubs.acs.org>.

AUTHOR INFORMATION

Corresponding Author

*E-mail: odedhod@tau.ac.il

Notes

The authors declare no competing financial interest.

ACKNOWLEDGMENTS

This work was supported by the Israel Science Foundation (ISF) under Grant No. 1313/08, the European Community's Seventh Framework Programme FP7/2007–2013 under Grant Agreement No. 249225, the Center for Nanoscience and Nanotechnology at Tel-Aviv University, and the Lise Meitner-Minerva Center for Computational Quantum Chemistry.

REFERENCES

- (1) Novoselov, K. S.; Geim, A. K.; Morozov, S. V.; Jiang, D.; Zhang, Y.; Dubonos, S. V.; Grigorieva, I. V.; Firsov, A. A. *Science* **2004**, *306* (5696), 666–669.
- (2) Berger, C.; Song, Z. M.; Li, X. B.; Wu, X. S.; Brown, N.; Naud, C.; Mayou, D.; Li, T. B.; Hass, J.; Marchenkov, A. N.; Conrad, E. H.; First, P. N.; de Heer, W. A. *Science* **2006**, *312* (5777), 1191–1196.
- (3) Han, M. Y.; Ozyilmaz, B.; Zhang, Y. B.; Kim, P. *Phys. Rev. Lett.* **2007**, *98* (20), 206805.
- (4) Cai, J. M.; Ruffieux, P.; Jaafar, R.; Bieri, M.; Braun, T.; Blankenburg, S.; Muoth, M.; Seitsonen, A. P.; Saleh, M.; Feng, X. L.; Mullen, K.; Fasel, R. *Nature* **2010**, *466* (7305), 470–473.
- (5) Hod, O.; Barone, V.; Peralta, J. E.; Scuseria, G. E. *Nano Lett.* **2007**, *7* (8), 2295–2299.
- (6) Stankovich, S.; Dikin, D. A.; Dommett, G. H. B.; Kohlhaas, K. M.; Zimney, E. J.; Stach, E. A.; Piner, R. D.; Nguyen, S. T.; Ruoff, R. S. *Nature* **2006**, *442* (7100), 282–286.
- (7) Schedin, F.; Geim, A. K.; Morozov, S. V.; Hill, E. W.; Blake, P.; Katsnelson, M. I.; Novoselov, K. S. *Nat. Mater.* **2007**, *6* (9), 652–655.
- (8) Barbulina, I. I.; Novoselov, K. S.; Morozov, S. V.; Dubonos, S. V.; Missous, M.; Volkov, A. O.; Christian, D. A.; Grigorieva, I. V.; Geim, A. K. *Appl. Phys. Lett.* **2006**, *88* (1), 013901.
- (9) Di, C. A.; Wei, D. C.; Yu, G.; Liu, Y. Q.; Guo, Y. L.; Zhu, D. B. *Adv. Mater.* **2008**, *20* (17), 3289–3293.
- (10) Kusakabe, K.; Maruyama, M. *Phys. Rev. B* **2003**, *67* (9), 092406.
- (11) Yamashiro, A.; Shimoj, Y.; Harigaya, K.; Wakabayashi, K. *Phys. Rev. B* **2003**, *68* (19), 193410.
- (12) Nakada, K.; Fujita, M.; Dresselhaus, G.; Dresselhaus, M. S. *Phys. Rev. B* **1996**, *54* (24), 17954–17961.
- (13) Fujita, M.; Wakabayashi, K.; Nakada, K.; Kusakabe, K. *J. Phys. Soc. Jpn.* **1996**, *65* (7), 1920–1923.
- (14) Son, Y. W.; Cohen, M. L.; Louie, S. G. *Nature* **2006**, *444* (7117), 347–349.
- (15) Gunlycke, D.; Li, J. W.; Mintmire, J. W.; White, C. T. *Nano Lett.* **2010**, *10* (9), 3638–3642.
- (16) Ramprasad, R.; von Allmen, P.; Fonseca, L. R. C. *Phys. Rev. B* **1999**, *60* (8), 6023–6027.
- (17) Cantele, G.; Lee, Y. S.; Ninno, D.; Marzari, N. *Nano Lett.* **2009**, *9* (10), 3425–3429.
- (18) Gunlycke, D.; Li, J.; Mintmire, J. W.; White, C. T. *Appl. Phys. Lett.* **2007**, *91* (11), 112108.
- (19) Huang, H.; Li, Z.; Wang, W. *J. Appl. Phys.* **2012**, *112* (11), 114332.
- (20) Huang, H.; Li, Z.; She, J.; Wang, W. *J. Appl. Phys.* **2012**, *111* (5), 054317.
- (21) He, C.; Wang, W. *J. Appl. Phys.* **2013**, *114* (7), 074305.
- (22) Son, Y. W.; Cohen, M. L.; Louie, S. G. *Phys. Rev. Lett.* **2006**, *97* (21), 216803.
- (23) Hod, O. *J. Chem. Theory Comput.* **2012**, *8* (4), 1360–1369.

- (24) Shi, Y. M.; Hamsen, C.; Jia, X. T.; Kim, K. K.; Reina, A.; Hofmann, M.; Hsu, A. L.; Zhang, K.; Li, H. N.; Juang, Z. Y.; Dresselhaus, M. S.; Li, L. J.; Kong, J. *Nano Lett.* **2010**, *10* (10), 4134–4139.
- (25) Song, L.; Ci, L. J.; Lu, H.; Sorokin, P. B.; Jin, C. H.; Ni, J.; Kvashnin, A. G.; Kvashnin, D. G.; Lou, J.; Yakobson, B. I.; Ajayan, P. M. *Nano Lett.* **2010**, *10* (8), 3209–3215.
- (26) Zeng, H. B.; Zhi, C. Y.; Zhang, Z. H.; Wei, X. L.; Wang, X. B.; Guo, W. L.; Bando, Y.; Golberg, D. *Nano Lett.* **2010**, *10* (12), 5049–5055.
- (27) Gorbachev, R. V.; Riaz, I.; Nair, R. R.; Jalil, R.; Britnell, L.; Belle, B. D.; Hill, E. W.; Novoselov, K. S.; Watanabe, K.; Taniguchi, T.; Geim, A. K.; Blake, P. *Small* **2011**, *7* (4), 465–468.
- (28) Tang, Q.; Zhou, Z.; Chen, Z. *J. Phys. Chem. C* **2011**, *115* (38), 18531–18537.
- (29) Nag, A.; Raidongia, K.; Hembram, K.; Datta, R.; Waghmare, U. V.; Rao, C. N. R. *ACS Nano* **2010**, *4* (3), 1539–1544.
- (30) Lin, Y.; Williams, T. V.; Xu, T. B.; Cao, W.; Elsayed-Ali, H. E.; Connell, J. W. *J. Phys. Chem. C* **2011**, *115* (6), 2679–2685.
- (31) Zhou, K. G.; Mao, N. N.; Wang, H. X.; Peng, Y.; Zhang, H. L. *Angew. Chem., Int. Ed.* **2011**, *50* (46), 10839–10842.
- (32) Bandyopadhyay, A.; Yamijala, S. S. R. K. C.; Pati, S. K. Tuning the electronic and optical properties of graphene and boron-nitride quantum dots by molecular charge-transfer interactions: a theoretical study. *Phys. Chem. Chem. Phys.* **2013**, *15* (33), 13881–13887.
- (33) Barone, V.; Peralta, J. E. *Nano Lett.* **2008**, *8* (8), 2210–2214.
- (34) Park, C. H.; Louie, S. G. *Nano Lett.* **2008**, *8* (8), 2200–2203.
- (35) Wu, X. J.; Wu, M. H.; Zeng, C. *Front. Phys. China* **2009**, *4* (3), 367–372.
- (36) Wang, Y. L.; Ding, Y.; Ni, J. *Phys. Rev. B* **2010**, *81* (19), 193407.
- (37) Chen, W.; Li, Y. F.; Yu, G. T.; Li, C. Z.; Zhang, S. B. B.; Zhou, Z.; Chen, Z. F. *J. Am. Chem. Soc.* **2010**, *132* (5), 1699–1705.
- (38) Yamijala, S.; Pati, S. K. *J. Phys. Chem. C* **2013**, *117* (7), 3580–3594.
- (39) Lopez-Bezanilla, A.; Huang, J. S.; Terrones, H.; Sumpter, B. G. *Nano Lett.* **2011**, *11* (8), 3267–3273.
- (40) Frisch, M. J.; Trucks, G. W.; Schlegel, H. B.; Scuseria, G. E.; Robb, M. A.; Cheeseman, J. R.; Scalmani, G.; Barone, V.; Mennucci, B.; Petersson, G. A.; Nakatsuji, H.; Caricato, M.; Li, X.; Hratchian, H. P.; Izmaylov, A. F.; Bloino, J.; Zheng, G.; Sonnenberg, J. L.; Hada, M.; Ehara, M.; Toyota, K.; Fukuda, R.; Hasegawa, J.; Ishida, M.; Nakajima, T.; Honda, Y.; Kitao, O.; Nakai, H.; Vreven, T.; Montgomery, J. A., Jr.; Peralta, J. E.; Ogliaro, F.; Bearpark, M.; Heyd, J. J.; Brothers, E.; Kudin, K. N.; Staroverov, V. N.; Kobayashi, R.; Normand, J.; Raghavachari, K.; Rendell, A.; Burant, J. C.; Iyengar, S. S.; Tomasi, J.; Cossi, M.; Rega, N.; Millam, J. M.; Klene, M.; Knox, J. E.; Cross, J. B.; Bakken, V.; Adamo, C.; Jaramillo, J.; Gomperts, R.; Stratmann, R. E.; Yazyev, O.; Austin, A. J.; Cammi, R.; Pomelli, C.; Ochterski, J. W.; Martin, R. L.; Morokuma, K.; Zakrzewski, V. G.; Voth, G. A.; Salvador, P.; Dannenberg, J. J.; Dapprich, S.; Daniels, A. D.; Farkas, O.; Foresman, J. B.; Ortiz, J. V.; Cioslowski, J.; Fox, D. J. *Gaussian 09*, revision A.02; Gaussian, Inc.: Wallingford, CT, 2009.
- (41) Perdew, J. P.; Burke, K.; Ernzerhof, M. *Phys. Rev. Lett.* **1996**, *77* (18), 3865–3868.
- (42) Perdew, J. P.; Burke, K.; Ernzerhof, M. *Phys. Rev. Lett.* **1997**, *78* (7), 1396–1396.
- (43) Heyd, J.; Scuseria, G. E.; Ernzerhof, M. *J. Chem. Phys.* **2003**, *118* (18), 8207–8215.
- (44) Heyd, J.; Scuseria, G. E.; Ernzerhof, M. *J. Chem. Phys.* **2006**, *124* (21), 219906.
- (45) Heyd, J.; Scuseria, G. E. *J. Chem. Phys.* **2004**, *120* (16), 7274–7280.
- (46) Heyd, J.; Scuseria, G. E. *J. Chem. Phys.* **2004**, *121* (3), 1187–1192.
- (47) Barone, V.; Hod, O.; Scuseria, G. E. *Nano Lett.* **2006**, *6* (12), 2748–2754.
- (48) Hod, O.; Peralta, J. E.; Scuseria, G. E. *Phys. Rev. B* **2007**, *76* (23), 233401.
- (49) Hod, O.; Scuseria, G. E. *ACS Nano* **2008**, *2* (11), 2243–2249.
- (50) Barone, V.; Hod, O.; Peralta, J. E.; Scuseria, G. E. *Acc. Chem. Res.* **2011**, *44* (4), 269–279.
- (51) Barone, V.; Hod, O.; Peralta, J. E. *Modeling of Quasi-One-Dimensional Carbon Nanostructures with Density Functional Theory* *Handbook of Computational Chemistry*; Leszczynski, J., Ed.; Springer: Netherlands, 2012; pp 901–938.
- (52) This basis set consists of (3s 2p 1d) contracted Gaussian functions for C and Li and (2s 1p) for H
- (53) We note that none of the DFT exchange-correlation functional approximations that we consider provide a full description of the long-range correlation effects required for the appropriate description of hydrogen bonding. Therefore, we expect that a proper inclusion of such effects will further increase the calculated relative stability of the OH(II) oxidation scheme.
- (54) Dumitrica, T.; Hua, M.; Yakobson, B. I. *Phys. Rev. B* **2004**, *70* (24), 241303.
- (55) We use a 68 k-point uniform grid for all calculations of the one-dimensional ZBNNRs studied.